World Journal of Radiology

Online Submissions: http://www.wjgnet.com/1949-8470office
wjr@wjgnet.com
doi:10.4329/wjr.v2.i6.215

World J Radiol 2010 June 28; 2(6): 215-223
ISSN 1949-8470 (online)

TOPIC HIGHLIGHT

Hui-Xiong Xu, MD, PhD, *Series Editor*

Computer-aided diagnosis for contrast-enhanced ultrasound in the liver

Katsutoshi Sugimoto, Junji Shiraishi, Fuminori Moriyasu, Kunio Doi

Katsutoshi Sugimoto, Junji Shiraishi, Kunio Doi, Kurt Rossmann Laboratories for Radiologic Imaging Research, Department of Radiology, The University of Chicago, Chicago, IL 60637, United States
Katsutoshi Sugimoto, Fuminori Moriyasu, Department of Gastroenterology and Hepatology, Tokyo Medical University, Tokyo 160-0023, Japan
Junji Shiraishi, School of Health Sciences, Kumamoto University, Kumamoto 862-0976, Japan
Author contributions: All authors analyzed and interpreted the data; Sugimoto K drafted the manuscript; Sugimoto K and Doi K researched the literature; Shiraishi J and Doi K edited the manuscript.
Correspondence to: Katsutoshi Sugimoto, MD, Department of Gastroenterology and Hepatology, Tokyo Medical University, Japan 6-7-1 Nishishinjuku, Shinjuku-ku, Tokyo 160-0023, Japan. sugimoto@tokyo-med.ac.jp
Telephone: +81-3-33426111 Fax: +81-3-53816654
Received: February 21, 2010 Revised: May 6, 2010
Accepted: May 13, 2010
Published online: June 28, 2010

Abstract

Computer-aided diagnosis (CAD) has become one of the major research subjects in medical imaging and diagnostic radiology. The basic concept of CAD is to provide computer output as a second opinion to assist radiologists' image interpretations by improving the accuracy and consistency of radiologic diagnosis and also by reducing the image-reading time. To date, research on CAD in ultrasound (US)-based diagnosis has been carried out mostly for breast lesions and has been limited in the fields of gastroenterology and hepatology, with most studies being conducted using B-mode US images. Two CAD schemes with contrast-enhanced US (CEUS) that are used in classifying focal liver lesions (FLLs) as liver metastasis, hemangioma, or three histologically differentiated types of hepatocellular carcinoma (HCC) are introduced in this article: one is based on physicians' subjective pattern classifications (subjective analysis) and the other is a computerized scheme for classification of FLLs (quantitative analysis). Classification accuracies for FLLs for each CAD scheme were 84.8% and 88.5% for metastasis, 93.3% and 93.8% for hemangioma, and 98.6% and 86.9% for all HCCs, respectively. In addition, the classification accuracies for histologic differentiation of HCCs were 65.2% and 79.2% for well-differentiated HCCs, 41.7% and 50.0% for moderately differentiated HCCs, and 80.0% and 77.8% for poorly differentiated HCCs, respectively. There are a number of issues concerning the clinical application of CAD for CEUS, however, it is likely that CAD for CEUS of the liver will make great progress in the future.

Key words: Computer-aided diagnosis; Focal liver lesion; Ultrasonography; Contrast agent; Micro-flow imaging

Peer reviewer: Juan Xu, PhD, University of Pittsburgh School of Medicine, UPMC Eye Center, 203 Lothrop St EEI- 835, Pittsburgh, PA 15213, United States

Sugimoto K, Shiraishi J, Moriyasu F, Doi K. Computer-aided diagnosis for contrast-enhanced ultrasound in the liver. *World J Radiol* 2010; 2(6): 215-223 Available from: URL: http://www.wjgnet.com/1949-8470/full/v2/i6/215.htm DOI: http://dx.doi.org/10.4329/wjr.v2.i6.215

INTRODUCTION

Ultrasound (US) is an easy-to-use and minimally invasive imaging modality that is useful for detection and qualitative diagnosis of focal liver lesions (FLLs). In addition, the detection and qualitative diagnosis of FLLs have been markedly improved by the development of US contrast agents consisting of microbubbles[1-5] and by harmonic imaging that can visualize nonlinear scattering of microbubbles[6-12].

It is well known that a major problem with US examinations is their operator-dependent nature, as compared with computed tomography (CT) and magnetic resonance (MR) imaging[13]. It is therefore necessary to reduce the operator-dependent limitations of US examinations. Computer-aided diagnosis (CAD) may be an approach that overcomes this problem.

To date, research on CAD in US-based diagnosis has been carried out mostly on breast lesions[14-19] and has been limited in the fields of gastroenterology and hepatology. In this article, we introduce CAD aimed at differential diagnosis of FLLs by use of contrast-enhanced US (CEUS), in addition to reviewing CAD on US in liver research.

WHAT IS CAD?

Recently, CAD has become a major research subject in medical imaging and diagnostic radiology[20-24]. Many different types of CAD schemes are being developed for the detection and/or characterization of lesions in various tissues using medical imaging, including conventional projection radiography, CT, MR imaging, and US. CAD research is being carried out on detecting lesions in breast, chest, colon, brain, liver and kidney, as well as the vascular and skeletal systems.

CAD is defined as a diagnosis made by a physician who takes into account the computer output based on quantitative analysis of radiologic images. This definition is clearly distinct from automated computerized diagnosis[25-27], which was attempted in the 1960s and 1970s and included replacing radiologists by computers. Subsequently, Doi *et al*[20-22] began their investigations on CAD at the University of Chicago in the 1980s with a clear goal of assisting radiologists with computerized information. The goal of CAD research is to improve the quality and productivity of radiologists' tasks by improving the accuracy and consistency of radiologic diagnoses and also by reducing the image-reading time.

CURRENT STATUS OF RESEARCH ON CAD BASED ON US OF THE LIVER

To date, CAD based on US of the liver has been frequently used in diffuse liver disease for quantifying the degree of liver fibrosis and fat deposition[28-30]. In addition, CAD for FLLs has been reported[31-34]; however, the number of such reports is small compared with the reports on CAD for diffuse liver disease. This is somewhat surprising because computers are, in general, superior to humans in quantitative measurements and in differential diagnosis, but inferior in lesion detection because of a large number of false positives. However, CAD has been used for quantitative evaluation of liver volume for support treatment, which included liver resection and radiofrequency ablation therapy applied to hepatocellular carcinoma (HCC) by application of volume measurements in 3D-US images[35,36]. All such applications have been developed based on B-mode US images.

Second-generation US contrast agents have been developed recently. Definity (Lantheus Inc., MA, USA) and SonoVue (Bracco, Milan, Italy) became available commercially in Canada and Europe, respectively, in 2001, whereas SonoVue became available in China in 2006, followed by Sonazoid (Daiichi Sankyo, Tokyo, Japan) in Japan in 2007 and SonoVue in Korea in 2008. Their utility for the diagnosis of FLLs has been reported[1-5]. In parallel, CAD with CEUS images for differentiating FLLs has been reported[33,34]. In these studies, FLLs were diagnosed by analysis of relatively simple blood flow parameters obtained from measurements of the time-intensity curve (TIC), which reflects tumor hemodynamics. Thus, research on CAD with CEUS images of the liver has just begun worldwide. In the next section, we introduce two different types of CAD schemes aimed at the differential diagnosis of FLLs, which were developed in collaboration with colleagues at the University of Chicago as examples of CAD[31,32].

SUBJECTIVE CLASSIFICATION OF FLLs USING PHYSICIANS' SUBJECTIVE PATTERN CLASSIFICATIONS (SUBJECTIVE ANALYSIS)

In this study, a total of 137 nodules in 137 cases were used for the development of CAD; specifically, there were 74 HCCs [23 well-differentiated (w-HCC), 36 moderately differentiated (m-HCC) and 15 poorly differentiated (p-HCC)], 33 liver metastases and 30 liver hemangiomas. HCC and liver metastasis were diagnosed based on histology after liver resection or liver biopsy in all cases. Liver hemangioma was diagnosed by contrast-enhanced CT and/or MR imaging. The US equipment used in this study was an SSA-790A (Aplio™XG; Toshiba Medical Systems Co., Otawara, Japan). The imaging mode was wideband harmonic imaging (commercially called Pulse subtraction) with transmission and reception frequencies of 3.75 MHz and 7.5 MHz, respectively. The contrast agent used was Sonazoid, which consists of perflubutane-based microbubbles surrounded by phospholipids with a median diameter of 2-3 μm.

From the baseline US features of an FLL, three experienced physicians were requested to classify the echogenic patterns of the FLL into one of the following eight patterns: (1) hyperechoic; (2) hypoechoic; (3) anechoic; (4) thin hypoechoic rim; (5) thick hypoechoic rim (bull's eye); (6) hyperechoic rim; (7) mosaic; and (8) others (Figure 1A). These patterns were proposed by Itai *et al*[37] for describing the characteristics of FLLs from baseline US.

After rating the echogenic patterns of FLLs from baseline US, the physicians were asked to classify the contrast-enhancement patterns of FLLs into one of the following eight patterns: (1) absent; (2) dotted; (3) peripheral rimlike; (4) peripheral nodular; (5) central with spoke wheel-shape; (6) diffuse heterogeneous; (7) diffuse homogeneous; and (8) others (Figure 1B). These patterns were proposed by

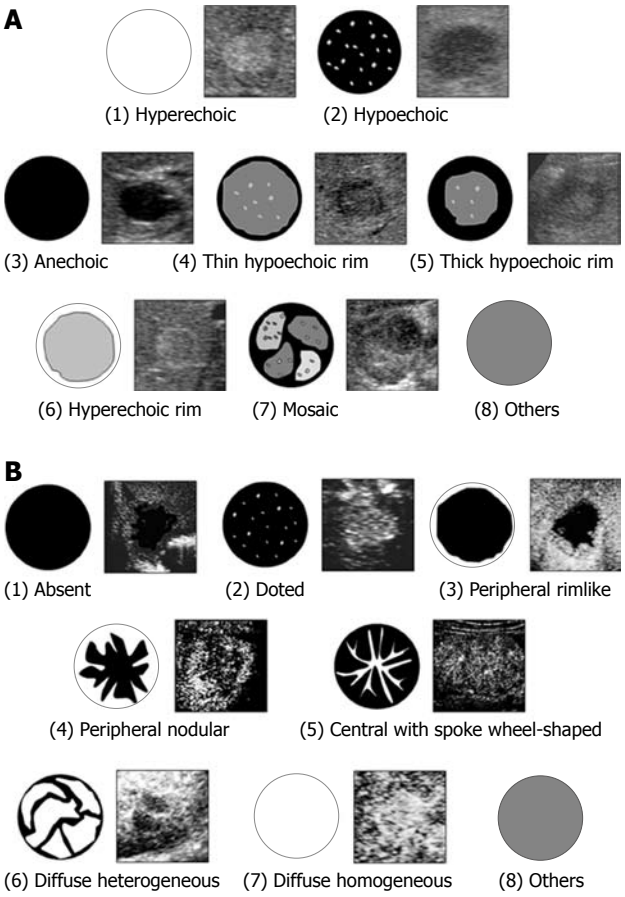

Figure 1 Hepatic tumors. A: Illustration of morphologic patterns of hepatic tumors in the B-mode ultrasonography; B: Illustration of enhancement patterns of hepatic tumors in the arterial phase.

Quaia *et al*[38]. The physicians were not asked to provide a diagnosis in this study.

For analysis of the subjective ratings obtained by the three physicians, we created a matrix of 137 FLLs and 16 patterns, which indicated the total number of physicians who rated lesions in each pattern.

To classify the five types of FLLs (i.e. w-HCCs, m-HCCs, p-HCCs, metastases and hemangiomas) in this CAD scheme, we employed four artificial neural networks (ANNs), as shown in Figure 2. ANNs are mathematical models based on biologic neural networks, which consist of an interconnected group of artificial neurons that can process information by using a connectionist approach to computation. The order of the four decisions (labeled D1-D4) in each ANN was determined by considering the diagnostic difficulty, which was based on the physicians' knowledge levels. The four decisions used in this study were the following: (1) D1: Is this lesion an HCC (yes) or other (no)? (2) D2: Is this lesion a hemangioma (yes) or metastasis (no)? (3)D3: Is this lesion a p-HCC (yes) or other HCC (no)? and (4) D4: Is this lesion a w-HCC (yes) or a m-HCC (no)?

All decisions were determined using each of the ANNs with a two-alternative choice method. In the learning and testing process of the ANNs, a leave-one-out test was employed in individual ANNs. In this method, one

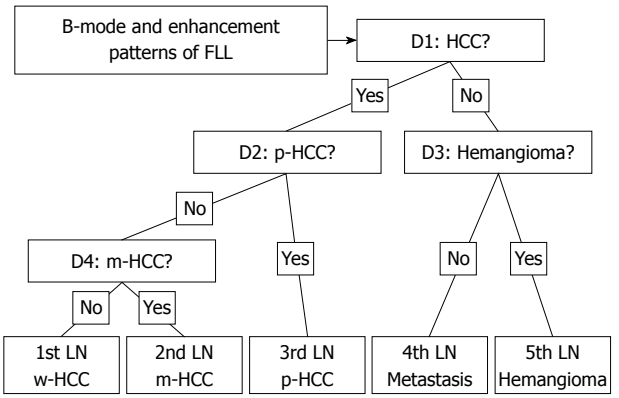

Figure 2 Illustration of the decision tree model used in this study. Four decision nodes in which alternative choice was determined by all five FLLs, leading to a final diagnostic decision for five liver lesions. D: Decision node; FLL: Focal liver lesion; HCC: Hepatocellular carcinoma; LN: Leaf node; m-HCC: Moderately differentiated HCC; p-HCC: Poorly differentiated HCC; w-HCC: Well-differentiated HCC.

case is left out for a test, and the ANN is trained to learn using the remaining cases. The one case that was left out is used for testing the trained ANN. The same procedure was then repeated until all cases were tested.

In the four ANNs, we did not use one of the subjective classifications (i.e. others), because we assumed that uncertain data might have a detrimental effect on the training of the ANNs. Thus, we used 14 input units corresponding to seven patterns of subjective classification data in the matrix as described previously.

The correct classification of the CAD scheme for the five types of FLLs was determined when the final outcome from the four ANNs agreed with the "gold standard". The classification accuracies for each type of FLL and also for all 137 FLLs were determined with the percentages of correctly classified cases among the total number of cases.

Table 1 shows the performance of the computerized scheme for the classification of the five types of FLLs. The classification accuracies for the 137 FLLs were 84.8% for metastasis, 93.3% for hemangioma, 65.2% for w-HCC, 41.7% for m-HCC, and 80.0% for p-HCC. When the classification was conducted only for three types of FLLs (i.e. HCCs, metastasis, and hemangioma), the classification accuracy for all HCCs was 98.6%, as shown in Table 2. The average classification accuracies for the three and five types of FLLs were 94.2% and 71.5%, respectively.

COMPUTERIZED SCHEME FOR CLASSIFICATION OF FLLs

Micro-flow imaging with contrast-enhanced ultrasonography

Micro-flow imaging (MFI; Toshiba Medical Systems Co., Otawara, Japan) is a novel image-processing technique that is accompanied by high-mechanical-index (MI > 1.0) disruptive flash frames and the maximum intensity projection (MIP) technique[32,39]. MIP processing is initi-

Table 1 Performance of CAD scheme for classification in five categories using physicians' pattern classification *n* (%)

Lesion	*n*	Classification with CAD				
		HCC			Metastasis	Hemangioma
		w-HCC	m-HCC	p-HCC		
HCC	74					
w-HCC	23	15 (65.2)	4 (17.4)	4 (17.4)	0 (0.0)	0 (0.0)
m-HCC	36	16 (44.4)	15 (41.7)	5 (13.9)	0 (0.0)	1 (2.7)
p-HCC	15	1 (6.7)	1 (6.7)	12 (80.0)	1 (6.7)	0 (0.0)
Metastasis	33	1 (3.0)	0 (0.0)	1 (3.0)	28 (84.8)	3 (9.1)
Hemangioma	30	0 (0.0)	0 (0.0)	1 (3.3)	1 (3.3)	28 (93.3)

Overall diagnostic accuracy: 98/137 (71.5%). CAD performance was evaluated by a leave-one-case-out methods. Reproduced, with modification, form Sugimoto *et al*[31], *Acad Radiol* 2009; 16: 401-411. CAD: Computer-aided diagnosis; HCC: Hepatocellular carcinoma; w-HCC: Well-differentiated HCC; m-HCC: Moderately differentiated HCC; p-HCC: Poorly differentiated HCC.

Table 2 Performance of CAD scheme for classification in three categories using physicians' subjective pattern classification *n* (%)

Lesion	*n*	Classification with CAD		
		HCC	Metastasis	Hemangioma
HCC	74	73 (98.6)	1 (1.4)	0 (0.0)
Metastasis	33	2 (6.1)	28 (84.8)	3 (9.1)
Hemangioma	30	1 (3.3)	1 (3.3)	28 (93.3)

Overall diagnostic accuracy: 129/137 (94.2%). CAD performance was evaluated by a leave-one-case out method. Reproduced, with modification, form Sugimoto *et al*[31], *Acad Radiol* 2009; 16: 401-411.

ated after a sonographic flash frame disrupts bubbles in the field of view. Using this technique, we could obtain information about the microbubble pathway between frames and observe exquisite detail of lesional vessels, with the potential to show both their morphology and their direction of filling[32,39,40].

To date, some investigators[39,41] have reported that the intratumoral vasculature of HCCs was clearly visualized using this technique and pattern classification was possible; these results suggested the possibility of differential diagnosis of the degree of HCCs[39,41]. CEUS with MFI could be useful for diagnosis of HCCs, and other FLLs, because MFI can depict the minute intratumoral vasculature of the tumor better than harmonic imaging. In this study, we therefore used various kinds of image features that can be derived from MFI findings as input data for the CAD.

Image database

A total of 103 nodules in 97 cases were used for the development of CAD. In more detail, there were 61 HCCs (24 w-HCC, 28 m-HCC and nine p-HCC), 26 liver metastases and 16 liver hemangiomas. HCCs and liver metastases were diagnosed based on histology after liver resection or liver biopsy in all cases. Liver hemangioma was diagnosed by contrast-enhanced CT and/or MR imaging. The US equipment used in this study was SSA-770A (Aplio™XV; Toshiba Medical Systems Co., Otawara, Japan). The imaging mode was wideband harmonic imaging (commercially called Pulse subtraction) with transmission and reception frequencies of 3.75 MHz and 7.5 MHz, respectively. The contrast agent we used was SonoVue, which consists of sulfur hexafluoride microbubbles surrounded by phospholipids with a median diameter of 2.5 μm.

Computerized scheme for classification of FLLs

A series of image-processing steps in CAD, which basically consisted of three major parts, were as follows: (1) image data input and construction of processed images; (2) extraction of image feature values; and (3) application of ANNs and output for differential diagnosis. Please note that we simplified into three major steps (although six major steps were described in the referenced paper[32]).

Image data input and construction of processed images: After irrelevant information, such as patient names, IDs, and other symbols, was removed from the cine clips in the audio-video interleaving format as the input data, only continuous MFI images were reconstructed, and then four kinds of processed images were constructed. Figure 3A-H shows examples of the processed images. Image feature values were determined by use of the MFI image and the four processed images, and were used as input data for the CAD.

Extraction of image feature values: The image feature value is defined as the objective value by computer analysis of the subjective criteria that are used for diagnosing an FLL accurately in clinical practice, such as quick (slow) contrast-enhancement of an FLL, stronger (weaker) contrast enhancement of an FLL compared with liver parenchyma, and homogeneous (heterogeneous) contrast-enhancement of an FLL. For example, with regard to the speed of contrast enhancement, changes in average pixel values in an FLL are plotted against the time axis, and the slope (β value) is calculated. The steeper the slope, the faster the speed of contrast enhancement would be. Similarly, the maximum level of the average pixel value is compared between an FLL and a liver parenchyma for determining which region showed stronger contrast enhancement.

In this study, four kinds of major image feature values were used as CAD input data. Their image characteristics were as follows: (1) temporal feature; (2) morpho-

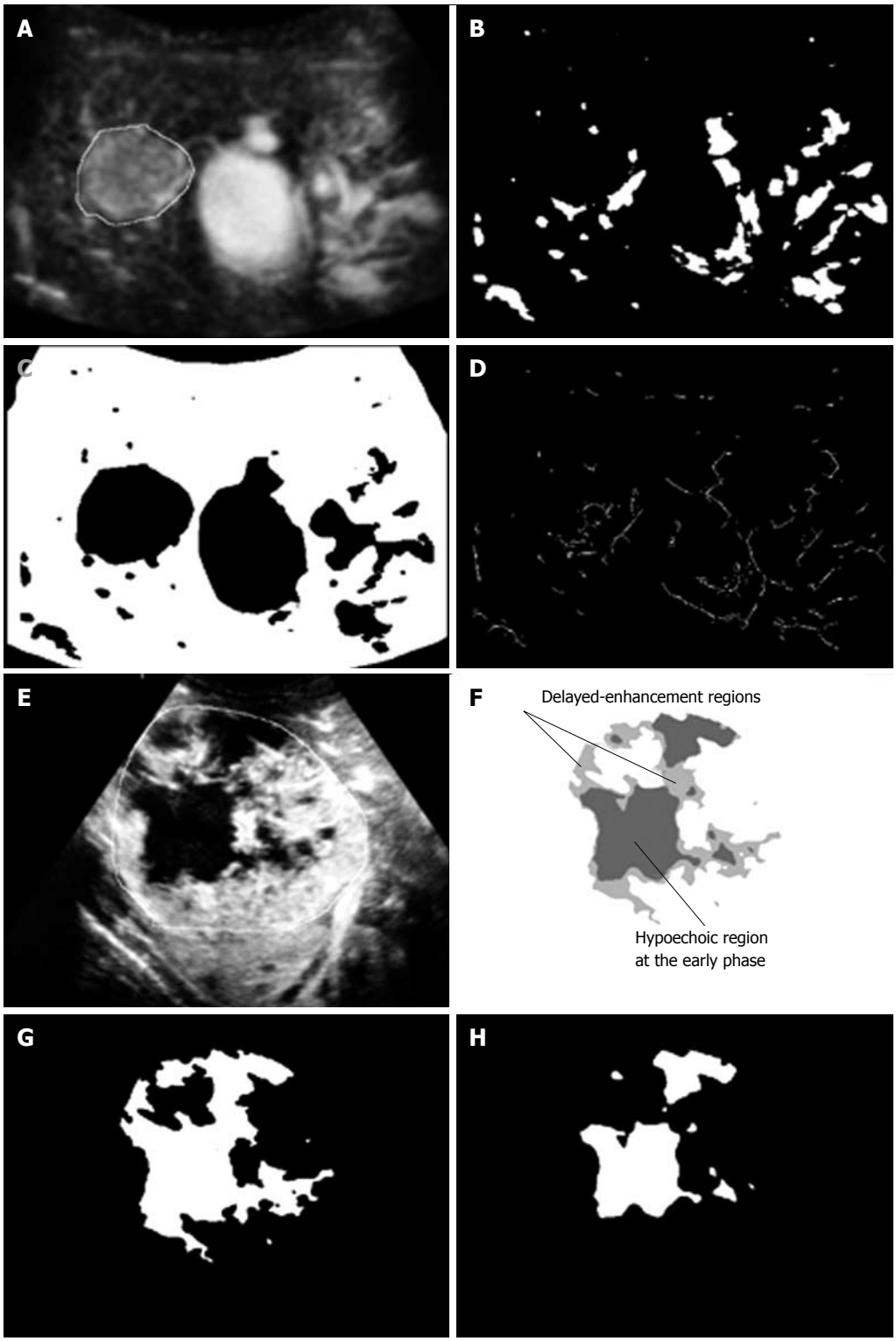

Figure 3 Extraction of morphologic and gray-level image features. A: Original MFI image at the early phase including one FLL (shown as the contour) and a portal vein; B: Vessel-like pattern enhanced image; C: Segmented adjacent liver parenchyma regions obtained from the original MFI image; D: Skeleton of vessel-like pattern enhanced image for estimating the average size of vessel-like patterns on the MFI image; Example of original MFI image at the delayed phase (E) and its segmented images for hyperechoic regions at the early (G) and delayed phase (H). The difference in the regions between two images at two phases was defined as delayed-enhancement region (F). Please note that we defined an "early phase" and a "delayed phase" in the MFI as a replenishment time for reaching 50% and 98% of the maximum average pixel value within a FLL, respectively. MFI: Micro-flow imaging. Reproduced, with modification, from Shiraishi *et al*[32], *Med Phys* 2008; 35: 1734-1746.

logic feature; (3) gray-level feature; and (4) features for a hypoechoic region. The details are shown in Table 3.

Feature 1 is an image feature value obtained from TIC, such as replenishment time, the peak pixel value, and the slope factor (β). In CEUS, for example, a hemangioma is characterized by a typical pattern, namely, a

Table 3 Image feature values used for CAD input data

Image feature values
Temporal features
Replenishment time (s)
Peak pixel value
Slope factor (β)
Morphologic features
Effective diameter of focal liver lesion
Average size of vessel-like patterns
Area ratio of vessel-like patterns
Gray-level features
Average pixel value with vessel-like patterns
Average pixel value without vessel-like patterns
Standard deviation of pixel value with vessel-like patterns
Standard deviation of pixel value without vessel-like patterns
Average pixel value ratio (focal liver lesion/adjacent liver parenchyma)
Average pixel value ratio (central/peripheral)
Features for hypoechoic region
Average pixel value
No. of hypoechoic regions
Area ratio of hypoechoic region
Difference in pixel value (delay-early)
Change in pixel value (delay-early)/s

Reproduced, with modification, from Shiraishi *et al*[32], *Med Phys* 2008; 35: 1734-1746.

peripheral globular enhancement with centripetal filling, whereas HCC and metastatic liver tumor are characterized by rapid contrast enhancement in an arterial phase. Use of the temporal feature as an image feature value, therefore, may be useful for differentiation of FLLs with different speeds of blood flow.

Feature 2 is an image feature value representing the morphologic characteristics of FLLs and intratumoral blood vessels, such as the effective diameter of an FLL, the average size of vessel-like patterns and the area ratio of vessel-like patterns. It has been reported that HCC with a larger tumor diameter exhibits poorer histological differentiation (i.e. higher percentages of p-HCC)[42], and thus the effective diameter of an FLL may be useful for diagnosis of histological grades of HCC. In addition, previous reports showed that the intratumoral vasculature visualized by MFI was dependent on the histological grade of HCC[39,41]. Thus, use of the morphologic image feature values obtained from the vessel-like pattern and the skeleton of a vessel-like pattern image may be useful for diagnosis of the histologic grade of HCC.

Feature 3 is an image feature value that represents tumor enhancement patterns, such as stronger contrast enhancement at the periphery of the tumor than at the center and at the tumor compared to the liver parenchyma. It has been reported that metastatic liver tumors often exhibit ring-like enhancement, and thus use of this image feature value may be useful for diagnosis of tumors with different contrast enhancement patterns.

Feature 4 is an image feature value that represents intratumoral heterogeneity in contrast enhancement. For example, spatial and temporal heterogeneity of a tumor in contrast enhancement can be evaluated by comparison

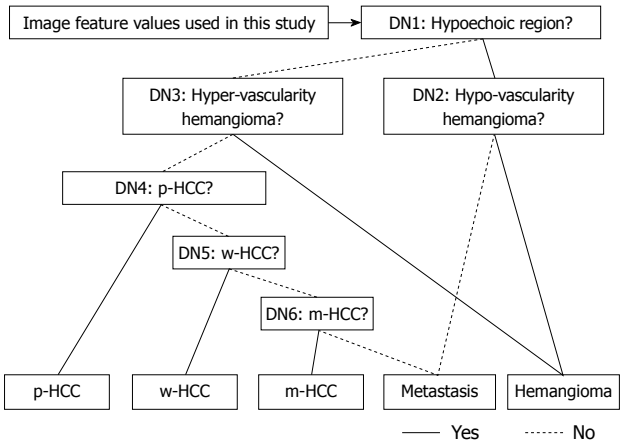

Figure 4 Illustration of the cascade of six artificial neural networks used in this. Six decisions in which alternative choices for specific groups of FLLs were determined by single ANN, leading a final diagnostic decision for five liver diseases.

of hypoechoic areas (no enhanced areas) between the MFI early-phase image and the MFI delayed-phase image. It has been reported that metastatic liver tumors and p-HCC often exhibit heterogeneous enhancement when compared with other liver tumors[38,43], and thus these image features may be useful for the differentiation of these tumors.

In order to select appropriate combinations of temporal and morphologic image features for each of the six ANNs, we used a stepwise method[44]. We thereby selected 16 temporal and morphologic image features, which were selected from 43 initial extracted features, and used them as input data for the six different ANNs for making decisions at each decision step in the cascade.

Application of ANNs and output for differential diagnosis: In the CAD, image feature values extracted from MFI images were used for input data for ANNs. We used parameters in the ANNs to learn the relationship between the repeated presentation of input data in random order and their corresponding output "teacher" data. Our ANNs were constructed with the stratified six different ANNs in order to classify "unknown" FLL input into one of five types of liver diseases (e.g. w-HCC, m-HCC, p-HCC, liver metastasis and liver hemangioma).

All decisions in each of the stratified six different ANNs, shown in Figure 4, were determined using a two-alternative choice. The six decisions used in the six ANNs were determined as follows: (1) D1: Does this lesion have hypoechoic regions (yes) or not (no)? (2) D2: Is this lesion a hypovascular hemangioma (yes) or a hypovascularity metastasis (no)? (3) D3: Is this lesion a hypervascular hemangioma (yes) or other (no)? (4) D4: Is this lesion a p-HCC (yes) or other (no)? (5) D5: Is this lesion a w-HCC (yes) or other (no)? and (6) D6: Is this lesion a m-HCC (yes) or a hypervascular metastasis (no)?

A set of image feature values was selected for each ANN, and learning processes and tests were carried out independently. In learning and testing tasks with ANNs,

Table 4 Performance of CAD scheme for classification in five categories using computerized scheme *n* (%)

Lesion	*n*	Classification with CAD				
		HCC			Metastasis	Hemangioma
		w-HCC	m-HCC	p-HCC		
Total	103					
w-HCC	24	19 (79.2)	1 (4.2)	2 (8.3)	2 (8.3)	0 (0.0)
m-HCC	28	5 (17.9)	14 (50.0)	4 (14.3)	3 (10.7)	2 (7.1)
P-HCC	9	1 (11.1)	0 (0.0)	7 (77.8)	1 (11.1)	0 (0.0)
Metastasis	26	2 (7.7)	1 (3.8)	0 (0.0)	23 (88.5)	0 (0.0)
Hemangioma	16	0 (0.0)	0 (0.0)	0 (0.0)	1 (6.3)	15 (93.8)

Overall diagnostic accuracy: 78/103 (75.7%). CAD performance was evaluated by a leave-one-case-out methods.Reproduced, with modification, from Shiraishi *et al*[32], *Med Phys* 2008; 35: 1734-1746.

the leave-one-out test method was employed in individual ANNs.

The classification accuracies for each type of FLL and also for all 103 FLLs were determined with percentages (%) of correctly classified cases among the total number of cases.

CAD results

Table 4 shows the performance of the computerized scheme for the classification of five types of FLLs (w-HCCs, m-HCCs, p-HCCs, metastases and hemangiomas). The classification accuracies for the 103 FLLs were 88.5% for metastasis, 93.8% for hemangioma, 79.2% for w-HCC, 50.0% for m-HCC and 77.8% for p-HCC. When the classification was done for three types of FLLs (HCCs, metastasis and hemangioma), the classification accuracies for all HCCs was 86.9%. The average classification accuracies for three and five types of FLLs were 88.3% and 75.7%, respectively.

PRACTICAL ISSUES IN CAD AND PERSPECTIVES FOR THE FUTURE

In general, a reliable image database is indispensable for research and development of CAD. In particular, an appropriate number of clinical cases should be used, and attention must be paid to the detection and/or characterization of lesions contained in the images and to the degrees of diagnostic difficulty. For development of a CAD scheme that will become available for clinical application, cases in the database should include various degrees of difficulty in diagnosis, from relatively easy to markedly difficult. Furthermore, the liver is the largest organ in the human body and part of the liver is protected by ribs. Unlike CT and MR imaging, it is therefore difficult to scan the whole liver by US[45]. In addition, US scanning can be difficult in cases of severe obesity. These factors seem to interfere with US on the liver, and also CAD for US on the liver.

One of the most critical components for research on CAD is software development. To this end, programming technology, image processing and knowledge of information processing are required. In general, however, physicians have insufficient knowledge of these skills, and thus close collaboration with physicists is required. On the other hand, it is difficult for software to be developed by physicists alone, because they have insufficient medical knowledge about diagnosis and detection. Therefore, close collaboration with physicians is also necessary.

As a characteristic of CAD, it would be useful if CAD could detect and/or characterize lesions that physicians are likely to overlook and/or misdiagnose, even if the performance of CAD is not highly accurate; and conversely, CAD would not be useful if physicians do not believe the results even when correct. Thus, once the algorithm of CAD is developed, its objective evaluation is necessary. To date, however, no paper on CAD in the liver has included an objective evaluation of the performance of CAD. An observer performance study is a representative evaluation method; observers are required to carry out evaluations under two conditions, with and without the results of computer analysis. Receiver operating characteristic curves can then be obtained based on the results for evaluation of the performance of CAD.

In addition, when the results of evaluation are satisfactory, based on the database in the laboratory, it is necessary to carry out practical tests on a number of unexplored clinical cases as the next step. It is also necessary to develop a practical CAD prototype system and to install it in the workplace in the hospital for a prospective clinical trial. To this end, cooperation by the hospital and physicians would be required for reliable evaluation.

Eventually, to reap the advantages of CAD, commercialization by companies is required. When equipment, systems and software applicable for clinical practice become available commercially, they can be used in hospitals worldwide.

CONCLUSION

In this article, we provided an overview of CAD based on US in the liver. Moreover, we introduced two different types of CAD schemes with CEUS images aimed at the differential diagnosis of FLLs.

The performance of our CAD system for the classification of FLLs could be considered as comparable to those reported by Wilson *et al*[9]. Although their report

was not on results of CAD, their algorithm used subjective assessment of physicians for information on portal venous enhancement for the distinction between benign and malignant FLLs, and their results indicated a high classification accuracy (i.e. 92% for benign and 93% for malignant FLLs).

As shown in this article, the diagnostic accuracies of CAD based on the results of physicians' subjective pattern classification could be considered as comparable to those of CAD based on a computerized scheme. Interestingly, the former CAD was, however, superior to the latter in the diagnosis of three types of FLLs (i.e. HCCs, metastasis, and hemangioma; 94.2% *vs* 88.3%). In contrast, the latter was superior to the former in the diagnosis of five types of FLLs (w-HCCs, m-HCCs, p-HCCs, metastases and hemangiomas; 75.7% *vs* 71.5%). These results suggest that human observers might differ in determining feature values from a computer in the diagnosis of FLLs. Thus, if we take advantage of computer outputs, diagnostic accuracy could be greatly improved.

In our present studies, to establish CAD for FLLs, we used temporal and morphologic features, including physicians' subjective pattern classifications, as image features of FLLs on the contrast-enhancement patterns in the arterial phase of CEUS. However, we did not use findings from portal and late phases (i.e. the presence or absence of washout) as image features of our CADs. That is because, as it is now, it is difficult to recognize automatically all of the data in a dynamic-imaging series for input data because of the problem of the timing of patient breath holding.

Our CAD results showed that the accuracy of m-HCC in both CADs was quite low (subjective analysis: 41.7% and quantitative analysis: 50.0%). This can be related to the fact that we did not use portal and late phase images as input data of CADs, because both w-HCC and m-HCC frequently show arterial enhancement in the same fashion. It is a principal limitation of our CADs. Thus, if our CAD schemes would have portal and late phase information, the performance of our CADs would be much more improved. Our future work should be to recognize hole ultrasonographic image data (i.e. wash-in and wash-out information) automatically as input data to the CAD system.

The other limitation is that focal nodular hyperplasia (FNH) and hepatocellular adenoma were not included in these studies. Both FNH and hepatic adenoma tend to have FLLs presenting a hypervascular pattern in the arterial phase, and it can be difficult to distinguish from HCC, liver metastasis, and hemangioma. However, Kim *et al*[46] reported that monitoring the direction of early arterial filling or the vascular morphology continuously by CEUS enable one to differentiate, to some extent, among FLLs with hypervascularity, including FNH, hemangioma, HCCs, or metastases. However, hepatic adenoma lacks characteristic features even with CEUS, and differentiation of hepatic adenoma from other plethoric FLLs has been reported to be difficult. Hepatocellular adenoma is rare tumor, and therefore it seems extremely rare for this tumor to become a subject of differential diagnosis.

ACKNOWLEDGMENTS

The authors are grateful to Mrs. Elisabeth Lanzl for improving the manuscript.

REFERENCES

1 **Kitzman DW**, Goldman ME, Gillam LD, Cohen JL, Aurigemma GP, Gottdiener JS. Efficacy and safety of the novel ultrasound contrast agent perflutren (definity) in patients with suboptimal baseline left ventricular echocardiographic images. *Am J Cardiol* 2000; **86**: 669-674
2 **Leen E**, Angerson WJ, Yarmenitis S, Bongartz G, Blomley M, Del Maschio A, Summaria V, Maresca G, Pezzoli C, Llull JB. Multi-centre clinical study evaluating the efficacy of SonoVue (BR1), a new ultrasound contrast agent in Doppler investigation of focal hepatic lesions. *Eur J Radiol* 2002; **41**: 200-206
3 **Krix M**, Kiessling F, Essig M, Herth F, Karcher A, Le-Huu M, Kauczor HU, Delorme S. Low mechanical index contrast-enhanced ultrasound better reflects high arterial perfusion of liver metastases than arterial phase computed tomography. *Invest Radiol* 2004; **39**: 216-222
4 **Maruyama H**, Matsutani S, Saisho H, Mine Y, Yuki H, Miyata K. Different behaviors of microbubbles in the liver: time-related quantitative analysis of two ultrasound contrast agents, Levovist and Definity. *Ultrasound Med Biol* 2004; **30**: 1035-1040
5 **Gaiani S**, Celli N, Piscaglia F, Cecilioni L, Losinno F, Giangregorio F, Mancini M, Pini P, Fornari F, Bolondi L. Usefulness of contrast-enhanced perfusional sonography in the assessment of hepatocellular carcinoma hypervascular at spiral computed tomography. *J Hepatol* 2004; **41**: 421-426
6 **Burns PN**, Wilson SR, Simpson DH. Pulse inversion imaging of liver blood flow: improved method for characterizing focal masses with microbubble contrast. *Invest Radiol* 2000; **35**: 58-71
7 **Albrecht T**, Hoffmann CW, Schettler S, Overberg A, Ilg M, von Behren PL, Bauer A, Wolf KJ. B-mode enhancement at phase-inversion US with air-based microbubble contrast agent: initial experience in humans. *Radiology* 2000; **216**: 273-278
8 **Kim AY**, Choi BI, Kim TK, Kim KW, Lee JY, Han JK. Comparison of contrast-enhanced fundamental imaging, second-harmonic imaging, and pulse-inversion harmonic imaging. *Invest Radiol* 2001; **36**: 582-588
9 **Wilson SR**, Burns PN. An algorithm for the diagnosis of focal liver masses using microbubble contrast-enhanced pulse-inversion sonography. *AJR Am J Roentgenol* 2006; **186**: 1401-1412
10 **Wilson SR**, Burns PN. Liver mass evaluation with ultrasound: the impact of microbubble contrast agents and pulse inversion imaging. *Semin Liver Dis* 2001; **21**: 147-159
11 **Eckersley RJ**, Chin CT, Burns PN. Optimising phase and amplitude modulation schemes for imaging microbubble contrast agents at low acoustic power. *Ultrasound Med Biol* 2005; **31**: 213-219
12 **Leavens C**, Williams R, Foster FS, Burns PN, Sherar MD. Golay pulse encoding for microbubble contrast imaging in ultrasound. *IEEE Trans Ultrason Ferroelectr Freq Control* 2007; **54**: 2082-2090
13 **Harvey CJ**, Blomley MJ, Eckersley RJ, Cosgrove DO, Patel N, Heckemann RA, Butler-Barnes J. Hepatic malignancies: improved detection with pulse-inversion US in late phase of enhancement with SH U 508A-early experience. *Radiology* 2000; **216**: 903-908
14 **Gruszauskas NP**, Drukker K, Giger ML, Chang RF, Sennett CA, Moon WK, Pesce LL. Breast US computer-aided diagnosis system: robustness across urban populations in South Korea and the United States. *Radiology* 2009; **253**: 661-671
15 **Drukker K**, Gruszauskas NP, Sennett CA, Giger ML. Breast US computer-aided diagnosis workstation: performance with a large clinical diagnostic population. *Radiology* 2008; **248**: 392-397
16 **Wu WJ**, Moon WK. Ultrasound breast tumor image comput-

er-aided diagnosis with texture and morphological features. *Acad Radiol* 2008; **15**: 873-880
17 **Shen WC**, Chang RF, Moon WK. Computer aided classification system for breast ultrasound based on Breast Imaging Reporting and Data System (BI-RADS). *Ultrasound Med Biol* 2007; **33**: 1688-1698
18 **Sahiner B**, Chan HP, Roubidoux MA, Hadjiiski LM, Helvie MA, Paramagul C, Bailey J, Nees AV, Blane C. Malignant and benign breast masses on 3D US volumetric images: effect of computer-aided diagnosis on radiologist accuracy. *Radiology* 2007; **242**: 716-724
19 **Chen CM**, Chou YH, Han KC, Hung GS, Tiu CM, Chiou HJ, Chiou SY. Breast lesions on sonograms: computer-aided diagnosis with nearly setting-independent features and artificial neural networks. *Radiology* 2003; **226**: 504-514
20 **Doi K**, Giger ML, Nishikawa RM, Hoffmann KR, MacMahon H, Schmidt RA, Chua KG. Digital radiography. A useful clinical tool for computer-aided diagnosis by quantitative analysis of radiographic images. *Acta Radiol* 1993; **34**: 426-439
21 **Doi K**, MacMahon H, Katsuragawa S, Nishikawa RM, Jiang Y. Computer-aided diagnosis in radiology: potential and pitfalls. *Eur J Radiol* 1999; **31**: 97-109
22 **Doi K**. Current status and future potential of computer-aided diagnosis in medical imaging. *Br J Radiol* 2005; **78** Spec No 1: S3-S19
23 **Abe H**, MacMahon H, Engelmann R, Li Q, Shiraishi J, Katsuragawa S, Aoyama M, Ishida T, Ashizawa K, Metz CE, Doi K. Computer-aided diagnosis in chest radiography: results of large-scale observer tests at the 1996-2001 RSNA scientific assemblies. *Radiographics* 2003; **23**: 255-265
24 **Gur D**, Zheng B, Fuhrman CR, Hardesty L. On the testing and reporting of computer-aided detection results for lung cancer detection. *Radiology* 2004; **232**: 5-6
25 **Lodwick GS**, Haun CL, Smith WE, Keller RF, Robertson ED. Computer diagnosis of primary bone tumors: a preliminary report. *Radiology* 1963; **80**: 273-275
26 **Meyers PH**, Nice CM Jr, Becker HC, Nettleton WJ JR, Sweeney JW, Meckstroth GR. Automated computer analysis of radiographic images. *Radiology* 1964; **83**: 1029-1034
27 **Winsberg F**, Elkin M, Macy J, Bordaz V, Weymouth W. Detection of radiographic abnormalities in mammograms by means of optical scanning and computer analysis. *Radiology* 1967; **89**: 211-215
28 **Li G**, Luo Y, Deng W, Xu X, Liu A, Song E. Computer aided diagnosis of fatty liver ultrasonic images based on support vector machine. *Conf Proc IEEE Eng Med Biol Soc* 2008; **2008**: 4768-4771
29 **Thijssen JM**, Starke A, Weijers G, Haudum A, Herzog K, Wohlsein P, Rehage J, De Korte CL. Computer-aided B-mode ultrasound diagnosis of hepatic steatosis: a feasibility study. *IEEE Trans Ultrason Ferroelectr Freq Control* 2008; **55**: 1343-1354
30 **Jeong JW**, Lee S, Lee JW, Yoo DS, Kim S. The echotextural characteristics for the diagnosis of the liver cirrhosis using the sonographic images. *Conf Proc IEEE Eng Med Biol Soc* 2007; **2007**: 1343-1345
31 **Sugimoto K**, Shiraishi J, Moriyasu F, Doi K. Computer-aided diagnosis of focal liver lesions by use of physicians' subjective classification of echogenic patterns in baseline and contrast-enhanced ultrasonography. *Acad Radiol* 2009; **16**: 401-411
32 **Shiraishi J**, Sugimoto K, Moriyasu F, Kamiyama N, Doi K. Computer-aided diagnosis for the classification of focal liver lesions by use of contrast-enhanced ultrasonography. *Med Phys* 2008; **35**: 1734-1746
33 **Huang-Wei C**, Bleuzen A, Olar M, Portalez D, Roumy J, Trillaud H, Tranquart F. Role of parametric imaging in contrast-enhanced sonography of hepatic focal nodular hyperplasia. *J Clin Ultrasound* 2006; **34**: 367-373
34 **Huang-Wei C**, Bleuzen A, Bourlier P, Roumy J, Bouakaz A, Pourcelot L, Tranquart F. Differential diagnosis of focal nodular hyperplasia with quantitative parametric analysis in contrast-enhanced sonography. *Invest Radiol* 2006; **41**: 363-368
35 **Ishizawa T**, Yamamoto T, Sekikawa T. The diagnostic values of measuring the liver volume in detecting occult hepatic metastases from colorectal cancer. *Hepatogastroenterology* 2007; **54**: 514-517
36 **Gilja OH**, Hausken T, Berstad A, Odegaard S. Measurements of organ volume by ultrasonography. *Proc Inst Mech Eng H* 1999; **213**: 247-259
37 **Itai Y**, Ohtomo K, Ohnishi S, Atomi Y, Itoh T, Fukuhisa K, Iinuma T. Ultrasonography of small hepatic tumors. *Radiat Med* 1987; **5**: 14-19
38 **Quaia E**, Calliada F, Bertolotto M, Rossi S, Garioni L, Rosa L, Pozzi-Mucelli R. Characterization of focal liver lesions with contrast-specific US modes and a sulfur hexafluoride-filled microbubble contrast agent: diagnostic performance and confidence. *Radiology* 2004; **232**: 420-430
39 **Sugimoto K**, Moriyasu F, Kamiyama N, Metoki R, Yamada M, Imai Y, Iijima H. Analysis of morphological vascular changes of hepatocellular carcinoma by microflow imaging using contrast-enhanced sonography. *Hepatol Res* 2008; **38**: 790-799
40 **Wilson SR**, Jang HJ, Kim TK, Iijima H, Kamiyama N, Burns PN. Real-time temporal maximum-intensity-projection imaging of hepatic lesions with contrast-enhanced sonography. *AJR Am J Roentgenol* 2008; **190**: 691-5
41 **Yang H**, Liu GJ, Lu MD, Xu HX, Xie XY. Evaluation of the vascular architecture of hepatocellular carcinoma by micro flow imaging: pathologic correlation. *J Ultrasound Med* 2007; **26**: 461-467
42 **Fan ZH**, Chen MH, Dai Y, Wang YB, Yan K, Wu W, Yang W, Yin SS. Evaluation of primary malignancies of the liver using contrast-enhanced sonography: correlation with pathology. *AJR Am J Roentgenol* 2006; **186**: 1512-1519
43 **Jang HJ**, Kim TK, Burns PN, Wilson SR. Enhancement patterns of hepatocellular carcinoma at contrast-enhanced US: comparison with histologic differentiation. *Radiology* 2007; **244**: 898-906
44 **Hocking RR**. The analysis and selection of variables in linear regression. *Biometrics* 1976; **32**: 1-49
45 **Sugimoto K**, Shiraishi J, Moriyasu F, Saito K, Doi K. Improved detection of hepatic metastases with contrast-enhanced low mechanical-index pulse inversion ultrasonography during the liver-specific phase of sonazoid: observer performance study with JAFROC analysis. *Acad Radiol* 2009; **16**: 798-809
46 **Kim TK**, Jang HJ, Burns PN, Murphy-Lavallee J, Wilson SR. Focal nodular hyperplasia and hepatic adenoma: differentiation with low-mechanical-index contrast-enhanced sonography. *AJR Am J Roentgenol* 2008; **190**: 58-66

S- Editor Cheng JX **L- Editor** Lutze M **E- Editor** Zheng XM